Scaffolding mechanism of arrestin-2 in the cRaf/MEK1/ERK signaling cascade

Changxiu Qu[a,b,c,1], Ji Young Park[d,1], Min Woo Yun[d,1], Qing-tao He[c], Fan Yang[e], Kiae Kim[d], Donghee Ham[d], Rui-rui Li[c], T. M. Iverson[f], Vsevolod V. Gurevich[f], Jin-Peng Sun[c,2], and Ka Young Chung[d,2]

[a]Department of Physiology and Pathophysiology, School of Basic Medical Sciences, Peking University, Beijing 100191, China; [b]Key Laboratory of Molecular Cardiovascular Science, Ministry of Education, Beijing 100191, China; [c]Key Laboratory Experimental Teratology of the Ministry of Education and Department of Biochemistry and Molecular Biology, Shandong University School of Medicine, Jinan 250012, China; [d]School of Pharmacy, Sungkyunkwan University, Suwon 16419, Republic of Korea; [e]Key Laboratory Experimental Teratology of the Ministry of Education, Department of Physiology, School of Basic Medical Sciences, Shandong University, Jinan 250012, China; and [f]Department of Pharmacology, Vanderbilt University, Nashville, TN 37232

Edited by David Baker, University of Washington, Seattle, WA, and approved June 28, 2021 (received for review December 24, 2020)

Arrestins were initially identified for their role in homologous desensitization and internalization of G protein–coupled receptors. Receptor-bound arrestins also initiate signaling by interacting with other signaling proteins. Arrestins scaffold MAPK signaling cascades, MAPK kinase kinase (MAP3K), MAPK kinase (MAP2K), and MAPK. In particular, arrestins facilitate ERK1/2 activation by scaffolding ERK1/2 (MAPK), MEK1 (MAP2K), and Raf (MAPK3). However, the structural mechanism underlying this scaffolding remains unknown. Here, we investigated the mechanism of arrestin-2 scaffolding of cRaf, MEK1, and ERK2 using hydrogen/deuterium exchange–mass spectrometry, tryptophan-induced bimane fluorescence quenching, and NMR. We found that basal and active arrestin-2 interacted with cRaf, while only active arrestin-2 interacted with MEK1 and ERK2. The ATP binding status of MEK1 or ERK2 affected arrestin-2 binding; ATP-bound MEK1 interacted with arrestin-2, whereas only empty ERK2 bound arrestin-2. Analysis of the binding interfaces suggested that the relative positions of cRaf, MEK1, and ERK2 on arrestin-2 likely facilitate sequential phosphorylation in the signal transduction cascade.

arrestin | ERK | scaffold | MEK | cRaf

The mitogen-activated protein kinase (MAPK) signaling cascade is an intracellular signaling pathway that is activated by diverse external stresses and regulates various cellular functions such as differentiation and proliferation (1). MAPK activation cascades consist of three components: MAPK kinase kinase (MAP3K), MAPK kinase (MAP2K), and MAPK. MAP3K phosphorylates and activates MAP2K, which in turn phosphorylates and activates MAPK (1, 2). In mammals, there are four distinct MAPK groups, ERKs (ERK1 and 2), JNKs (JNK1, 2, and 3), p38 (p38α through δ), and ERK5, each of which has its own upstream MAP3Ks and MAP2Ks (2, 3).

A long-standing question in biochemistry is how diverse input signals can generate a specific MAPK signaling cascade. In other words, it is unknown how MAPK signaling modules dynamically interact in a spatiotemporal manner. To accomplish signaling fidelity, scaffolding proteins play an important role in colocalizing MAPK signaling modules. MAPK scaffolding proteins facilitate activation, regulate subcellular localization, and/or modulate the negative feedback of a specific MAPK signaling, which helps to organize a specific MAPK module to link the input signaling to proper biological outcomes (4, 5). Owing to the diverse roles of MAPK scaffolding proteins, they have been considered as potential therapeutic targets (6, 7).

In mammals, a number of MAPK scaffolding proteins, including JIP, KSR, paxillin, MORG1, JSAP1, and arrestins, have been identified (8, 9). The functional role of MAPK scaffolding and the molecular and structural mechanisms of how the MAPK scaffolding proteins interact with MAPK signaling components vary depending on the scaffolding proteins (4). Therefore, it is important to study the details of the scaffolding mechanism of each MAPK scaffolding protein to gain a better understanding of the MAPK signaling mechanism and to precisely regulate a specific MAPK signaling pathway for therapeutic purposes.

Arrestins were first discovered as proteins that play a key role in homologous desensitization and internalization of G protein–coupled receptors (GPCRs) (10). Four arrestins (arrestin-1 through -4) have been identified in humans: arrestin-1 and -4 (visual and cone arrestins, respectively) are expressed exclusively in the visual system, whereas arrestin-2 and -3 (also known as β-arrestin1 and 2, respectively) are ubiquitously expressed (10). Agonist-activated GPCRs, after coupling with G proteins, are phosphorylated by GPCR kinases. Arrestins bind active phosphorylated GPCRs, precluding receptor coupling to G proteins and facilitating receptor internalization (10, 11). In GPCR internalization, arrestins act as scaffolding proteins, linking the receptor with components of internalization machinery, such as clathrin and AP-2 (11–15). Arrestins have also been reported to interact with numerous signaling proteins, including MAPKs, and perform multiple functions (16, 17). The interaction with these signaling proteins occurs either in the basal or GPCR-induced active state of arrestins (11, 15, 18).

Arrestins are the only known scaffolding proteins for MAPKs that are regulated by GPCRs. The interaction between MAPKs and arrestins has been extensively studied (11, 15, 19–21). Arrestins regulate GPCR-mediated ERK1/2 activation by scaffolding cRaf-1, MEK1, and ERK1/2 (22, 23) and regulate

Significance

In addition to desensitizing and internalizing G protein–coupled receptors, arrestins mediate ERK1/2 activation by scaffolding three kinases: ERK1/2, MEK1, and Raf. The structural mechanism by which arrestins scaffold the ERK1/2 signaling cascade remains undetermined. Here, we investigated the mechanism of arrestin-2 scaffolding of the cRaf-MEK1-ERK2 signaling module. We identified the binding interfaces of arrestin-2 and these three kinases. We found that the binding of ERK2 and MEK1 was affected by the activation status of arrestin-2, and its interactions with MEK1 and ERK2 were affected by ATP. These results provide insights into the general scaffolding mechanism of the ERK1/2 cascade.

Author contributions: J.-P.S. and K.Y.C. designed research; C.Q., J.Y.P., M.W.Y., Q.-t.H., F.Y., K.K., R.-r.L., J.-P.S., and K.Y.C. performed research; J.-P.S. and K.Y.C. contributed new reagents/analytic tools; C.Q., J.Y.P., M.W.Y., K.K., D.H., J.-P.S., and K.Y.C. analyzed data; and C.Q., J.Y.P., M.W.Y., T.M.I., V.V.G., J.-P.S., and K.Y.C. wrote the paper.

The authors declare no competing interest.

This article is a PNAS Direct Submission.

[1]C.Q., J.Y.P., and M.W.Y. contributed equally to this work.

[2]To whom correspondence may be addressed. Email: kychung2@skku.edu or sunjinpeng@sdu.edu.cn.

This article contains supporting information online at https://www.pnas.org/lookup/suppl/doi:10.1073/pnas.2026491118/-/DCSupplemental.

Published September 10, 2021.

GPCR-dependent or -independent JNK3 signaling by scaffolding ASK1, MKK4/7, and JNK3 (24–26). Although the cellular and physiological effects of arrestins in MAPK signaling cascades have been studied extensively, the structural mechanisms governing arrestin/MAPK interactions have not been fully elucidated. Only a few studies have suggested a scaffolding mechanism of arrestins for ERK1/2 and JNK3 signaling components. A molecular simulation approach has suggested the binding interfaces of GPCR, arrestin-2, cSrc, cRaf, MEK1, and ERK1 (27), and mutation or truncation studies have investigated the interaction sites between arrestin and ERK1/2 signaling components (22, 28). Recent studies suggested an arrestin-3-mediated scaffolding and signal amplification mechanism of the JNK3 cascade (26, 29).

Here, we studied the interaction of ERK1/2 signaling cascade components (cRaf, MEK1, and ERK2) with arrestin-2 using a combination of hydrogen/deuterium exchange–mass spectrometry (HDX-MS), Trp-induced bimane fluorescence quenching, and NMR spectroscopy. HDX-MS measures the exchange rate between the hydrogen atoms of amides in the protein backbone and the deuterium atoms in the solvent, which can provide an insight into protein–protein binding interfaces (30). NMR and Trp-induced bimane fluorescence quenching enable the detailed mapping of interaction interfaces within proteins (29, 31).

Results

Binding between Arrestin-2 and ERK2. Arrestins are composed of N and C domains, and the C-terminal tail, including β-strand XX (Fig. 1*A*, yellow), is anchored to the N domain. Structural studies have revealed the binding interfaces between arrestins and receptors and the conformational changes in arrestins upon activation. A phosphorylated receptor C terminus interacts with several phosphate-binding residues in the N domain of arrestins, displacing β-strand XX (Fig. 1*A* and *SI Appendix*, Fig. S1*A*) (32–35). The loops in the middle of the receptor-binding side of arrestin interact with the receptor cytosolic core (*SI Appendix*, Fig. S1*A*) (32, 33, 35–37). The receptor-induced conformation of the active arrestins exhibits a characteristic interdomain rotation (*SI Appendix*, Fig. S1*B*), which involves the disruption of ionic interactions between the two domains (polar core; *SI Appendix*, Fig. S1*C*) (37, 38). Various studies have confirmed that removal of the C-terminal tail or disruption of the polar core results in the preactivation of arrestins, such that the arrestin conformational equilibrium is shifted toward the active state (39, 40).

To identify the binding interfaces between arrestin-2 and ERK2, we compared the HDX-MS profiles of arrestin-2 alone, ERK2 alone, and coincubated arrestin-2/ERK2. We also generated a C-terminally truncated preactivated arrestin-2 (arrestin-$2^{1–384}$) to test whether the activation status of arrestin-2 affects its interaction with ERK2 (Fig. 1*A*). The HDX-MS results are summarized in Datasets S1 and S2. We found that coincubation of ERK2 with wild-type (WT) arrestin-2 did not alter the HDX-MS profiles. In contrast, coincubation of ERK2 with arrestin-$2^{1–384}$ induced changes in the HDX-MS profile compared with ERK2 or arrestin-$2^{1–384}$ alone (Fig. 1 *B* and *C* and *SI Appendix*, Fig. S2*A*). The requirement for arrestin-2 activation for ERK2 binding was confirmed in cellular studies using a bioluminescence resonance energy transfer (BRET) assay. The binding between arrestin-2 and ERK2 increased when the cells were activated by angiotensin II (*SI Appendix*, Fig. S3*A*). Interestingly, we observed that the HDX-MS profile was altered only when arrestin-$2^{1–384}$ was incubated with empty ERK2 but not with ERK2 bound to the ATP analog (AMP-PNP) (Table 1). These results suggest that activated arrestin-2 interacts with ERK2 prior to the entry of ATP into its binding pocket.

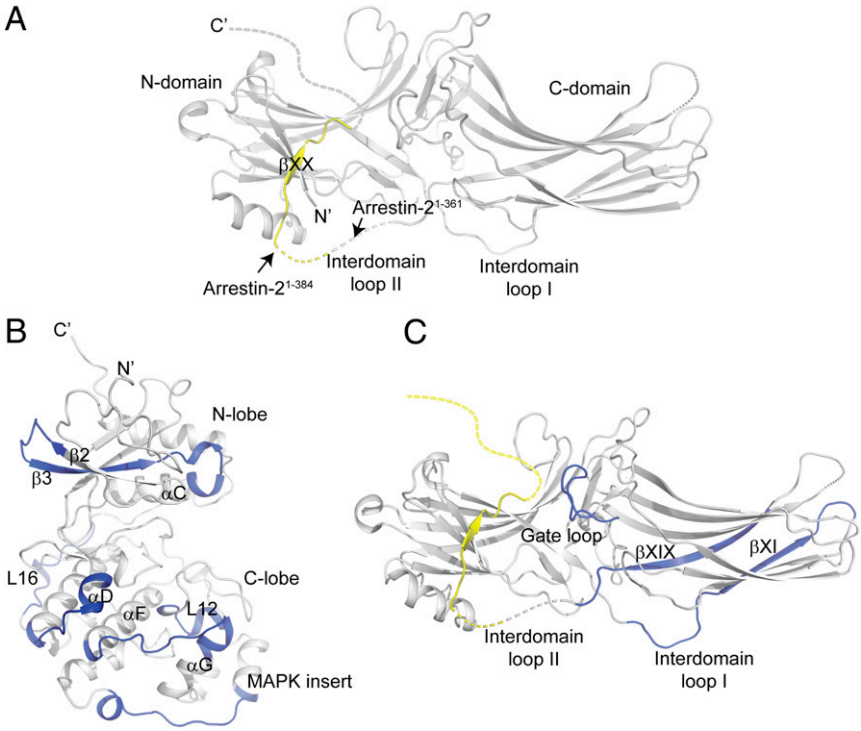

Fig. 1. Changes in HDX profile upon coincubation of ERK2 and arrestin-2. (*A*) The arrestin-2 constructs used in this study are shown on the X-ray crystal structure of bovine arrestin-2 (Protein Data Bank (PDB) ID: 1G4R). The C-terminal truncation positions are indicated with arrows. β-strand XX is shown in yellow. (*B*) Changes in the HDX profile of apo-ERK2 upon coincubation with arrestin-$2^{1–384}$. Regions with reduced HDX are colored blue on the X-ray crystal structure of ERK2 (PDB: 1ERK). The deuterium uptake plots with reduced HDX are shown in *SI Appendix*, Fig. S2*A*. (*C*) Changes in the HDX profile of arrestin-$2^{1–384}$ upon coincubation with apo-ERK2. Regions with reduced HDX are colored blue on the X-ray crystal structure of bovine arrestin-2 (PDB: 1G4R). The deuterium uptake plots with reduced HDX are shown in *SI Appendix*, Fig. S2*A*.

Table 1. HDX-MS profile changes upon coincubation

	ERK2		MEK1		cRaf RBD
	w/o ANP-PMP	w/ ANP-PMP	w/o ANP-PMP	w/ ANP-PMP	—
Basal arrestn-2	n.a	n.a	n.a	n.a	O
Preactivated arrestin-2	O	n.a	n.a	O	O

O: HDX-MS profiles were affected upon coincubation of arrestin-2 and ERK2 signaling components. n.a: HDX-MS profiles were not affected upon coincubation of arrestin-2 and ERK2 signaling components.

Coincubation of arrestin-$2^{1–384}$ resulted in decreased HDX in both the N- and C-lobes of ERK2 (Fig. 1*B* and *SI Appendix*, Fig. S2*A*; peptides 43 to 65, 113 to 124, 193 to 200, 222 to 237, 265 to 278, and 316 to 326). These regions include L3 through αC within the N-lobe, and αD through αE, L12, αF through αG (MAPK insert) and L16 within the C-lobe. Coincubation with ERK2 decreased HDX levels mostly in the C domain of arrestin-2, including the interdomain loop I through β-strand XI, the gate loop, and β-strand XIX through the interdomain loop II (Fig. 1*C* and *SI Appendix*, Fig. S2*A*; peptides 176 to 192, 290 to 300, and 343 to 365). The reduction in HDX upon coincubation of the two proteins reflects reduced solvent exposure, which suggests binding interfaces. However, HDX-MS data do not unambiguously identify the exact binding interface between the two proteins, as the HDX levels are also affected by the stability of the hydrogen bonds within the secondary structures such as helices and β-sheets.

To compensate for the limitations of HDX-MS data, we used Trp-induced bimane fluorescence quenching. When tryptophan is located near the bimane probe, bimane fluorescence is attenuated; thus, the relative distance between tryptophan and bimane-labeled residues can be monitored by measuring bimane fluorescence intensity (31). We incorporated tryptophan into selected positions in ERK2 (V49W, Y64W, Y113W, H125W, F228W/Y233W, and L267W), where we observed reduced HDX upon coincubation with arrestin-$2^{1–384}$ (Fig. 2*A*, purple sticks). We also mutated the solvent-exposed cysteine residues in arrestin-$2^{1–384}$ (details are described in the *Materials and Methods* section), incorporated cysteines at positions 300 and 356, where we observed reduced HDX upon ERK coincubation, and labeled these residues with monobromo-bimane (L300C_Arr2 and P356C_Arr2; Fig. 2*B*, orange sticks). These mutants did not affect the interaction between the ERK2 and Arr2, suggesting their functional integrity (*SI Appendix*, Fig. S4*A*).

The bimane fluorescence of L300C_Arr2 was not altered by coincubation with Y113W or F228W/Y233W ERK2 (Fig. 2*C*). In contrast, V49W, Y64W, H125W, and L267W ERK2 reduced bimane fluorescence in L300C_Arr2 compared to that upon coincubation with WT ERK2 (Fig. 2*C*). V49W and Y64W most significantly affected the bimane fluorescence in L300C_Arr2, suggesting that the gate loop of arrestin-2 is close to the ERK2 N-lobe.

The bimane fluorescence of P356C_Arr2 was reduced upon coincubation with Y113W, H125W, F228W/Y233W, and L267W ERK2 but not with V49W and Y64W (Fig. 2*D*). Interestingly, the bimane fluorescence of P356C_Arr2 was reduced, even upon coincubation with WT ERK2, compared with the buffer control (Fig. 2*D*). These observations may be due to the two intrinsic tryptophan residues within the C-lobe of ERK2 (Fig. 2*A*, cyan sticks). These data suggest that the interdomain loop II of arrestin-2 is close to the C-lobe of ERK2. Interestingly, interdomain loop II is more exposed when the C-terminal tail of arrestin-2 is released upon activation (*SI Appendix*, Fig. S1*A*). Change in the HDX-MS profile was observed only when ERK2 was coincubated with C-terminally truncated preactivated arrestin-2. Therefore, it is tempting to speculate that interdomain loop II is more exposed in the C-terminally truncated preactivated arrestin-2, which facilitates the interaction of interdomain loop II with the C-lobe of ERK2.

A previous report by Cassier et al. also suggested the involvement of interdomain loop II of arrestin in ERK interaction, suggesting that the phosphorylation of threonine 383 on interdomain loop II of arrestin-3 induced a conformational change in this region (41). This conformational change promotes the binding of phosphorylated C terminus of a receptor to the N domain of arrestin-3, the conversion of arrestin to its active conformation, and subsequent ERK binding (41). To investigate the role of interdomain loop II of arrestin-2 in the interaction with ERK2, we further truncated the C-terminal part to generate arrestin-$2^{1–361}$, which lacks the C-terminal part of the interdomain loop II (Fig. 1*A*). Unlike arrestin-$2^{1–384}$, coincubation of ERK2 and arrestin-$2^{1–361}$ did not alter HDX profiles in either ERK2 or arrestin-$2^{1–361}$, suggesting that ERK2 did not bind to arrestin-$2^{1–361}$. This supports interdomain loop II as one of the critical binding sites for ERK2.

To provide further structural insights into the interaction between ERK2 and arrestin-2, we incorporated unnatural amino acids into the gate loop or interdomain loop II: 4-trimethylsilyl phenylalanine (TMSF) and 3,5-difluorotyrosine (F2Y) at positions 300 (300TMSF) and 362 (362F2Y), respectively, using the genetic code expansion approach (details are described in the *Materials and Methods* section). We employed ^{1}H-NMR and ^{19}F-NMR spectroscopy to monitor ERK2 binding-induced conformational changes in arrestin-2. A notable upfield NMR shift at the 300TMSF site was observed upon coincubation with ERK2 (Fig. 2*E*), suggesting a localized increase in the electronic field at this position, likely due to interaction with the negatively charged residues in ERK2. On the other hand, a downfield NMR shift at the 362F2Y site was observed upon coincubation with ERK2 (Fig. 2*F*), suggesting a localized decrease in the electronic field at this position, likely due to the interaction with the positively charged residues in ERK2. The surface charge distribution of ERK2 revealed that positive surface charges are localized within the C-lobe, where we observed reduced HDX (Fig. 2 *A* and *G*).

Collectively, these results suggest that activated arrestin-2 interacts with ERK2, which is not bound to ATP, and uses two binding interfaces: 1) between the gate loop of arrestin-2 and the N-lobe of ERK2, and 2) between the interdomain loop II of arrestin-2 and the C-lobe of ERK2.

Binding between Arrestin-2 and MEK1. After identifying the binding interfaces between arrestin-2 and ERK2, we sought to localize the binding interfaces between arrestin-2 and MEK1, the MAP2K of the ERK1/2 activation pathway. To this end, we used another version of preactivated arrestin-2, R169E, in which the polar core is disrupted by charge reversal (42–44). In contrast to truncated arrestins, which lack the C-terminal tail, polar core disruption destabilizes the interdomain orientation, which shifts the equilibrium toward the active conformation (39, 42, 44). This variant is not as strongly activating but has advantages for this study because of the retention of the C-terminal tail in the R169E mutant, which can serve as a binding site.

When we coincubated R169E with empty MEK1, no changes in the HDX profile were detected. However, when we coincubated R169E with AMP-PNP-liganded MEK1, reduced HDX

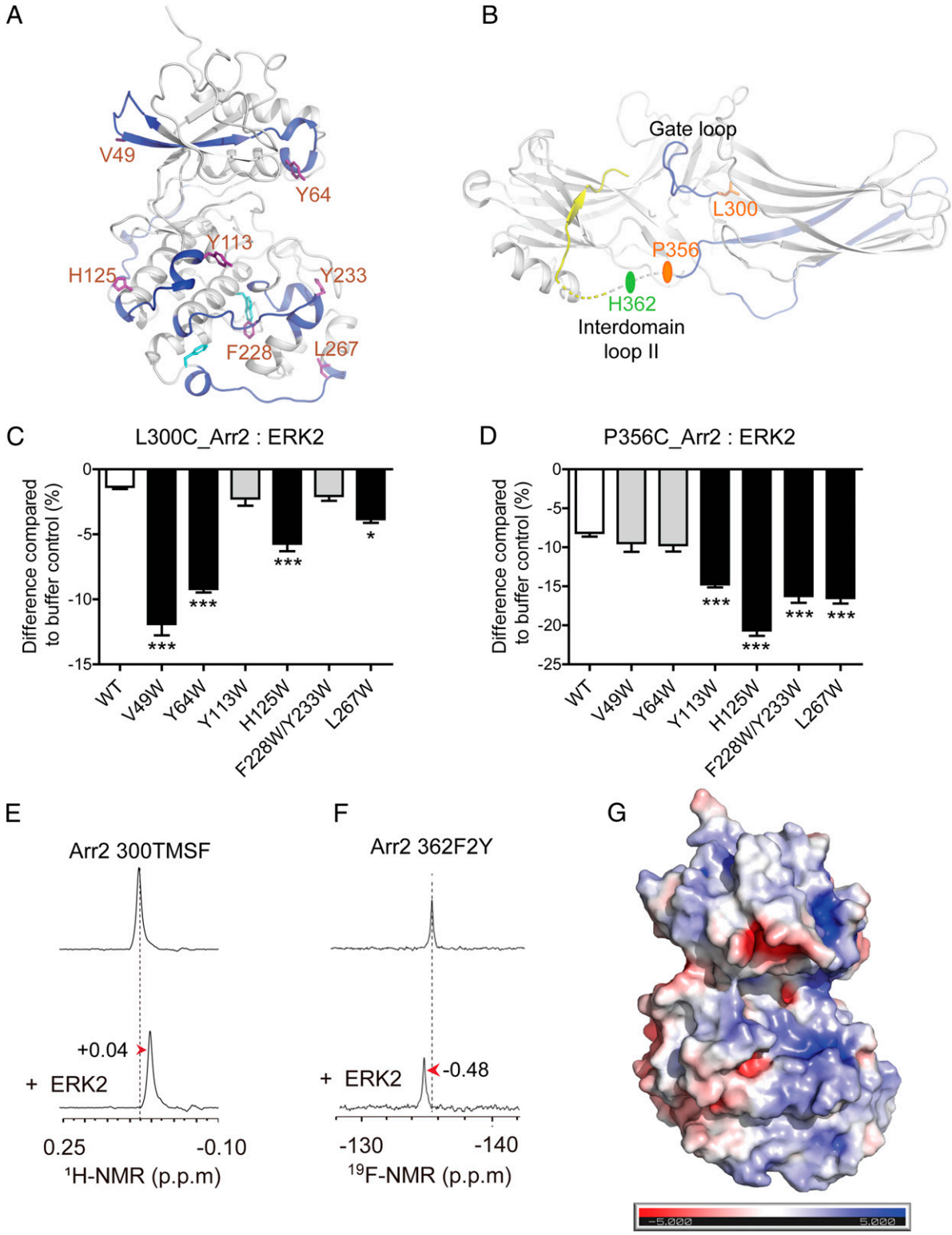

Fig. 2. Interaction of ERK2 and arrestin-2$^{1–384}$ detected by Trp-induced bimane fluorescence quenching, ^{1}H-NMR, and ^{19}F-NMR. (*A*) Positions of incorporated tryptophan in ERK2 are shown by purple sticks, and endogenous tryptophan is shown by cyan sticks on the X-ray crystal structure of ERK2 (PDB: 1ERK). Regions with reduced HDX in Fig. 1*B* are colored blue. (*B*) Positions of bimane-labeled cysteines and unnatural amino acid residues in arrestin-2$^{1–384}$ are shown in orange or green on the X-ray crystal structure of bovine arrestin-2 (PDB: 1G4R). Regions with reduced HDX in Fig. 1*C* are colored blue, and β-strand XX is colored yellow. (*C* and *D*) Quenching of bimane fluorescence [attached to Cys in L300C_Arr2 (*C*) or in P356C_Arr2 (*D*)] by Trp in apo-ERK2. Data are from three independent experiments. Error bars indicate SEM. Black bars indicate statistically significant differences from WT, and gray bars indicate the absence of statistically significant differences from WT. *$P < 0.05$, **$P < 0.01$, and ***$P < 0.001$ compared WT. (*E* and *F*) Effects of ERK2 binding on the ^{1}H-NMR spectrum of 300TMSF (*E*) and ^{19}F-NMR spectrum of 362F2Y (*F*) incorporated into arrestin-2$^{1–384}$. (*G*) Surface charge distribution of ERK2. The surface charge was analyzed with adaptive Poisson-Boltzmann solver (APBS) electronics, a PyMOL plugin program, using the ERK2 crystal structure (PDB: 1ERK).

https://doi.org/10.1073/pnas.2026491118

levels were detected in several regions of both MEK1 and R169E (Fig. 3 *A* and *B*, blue ribbon, and *SI Appendix*, Fig. S2*B*). The HDX-MS results are summarized in Datasets S1 and S3. Coincubation with R169E reduced HDX in the N-terminal region (peptide 53 to 68) and glycine-rich loop (peptide 75 to 83) of the N-lobe of MEK1 (Fig. 3*A* and *SI Appendix*, Fig. S2*B*). Coincubation with MEK1 reduced HDX levels at interdomain loop I, β-strand XVI through the lariat loop, and the gate loop in R169E (Fig. 3*B* and *SI Appendix*, Fig. S2*B*). In contrast, coincubation of WT arrestin-2 and AMP-PNP-liganded MEK1 did not alter HDX profiles (Table 1), suggesting that arrestin-2 needs to be activated to interact with MEK1. The requirement for arrestin-2 activation was confirmed in cellular studies using the BRET assay, which showed that the binding between arrestin-2 and MEK1 was increased when the cells were activated by angiotensin II (*SI Appendix*, Fig. S3*B*).

To identify the regions that serve as the binding sites for MEK1, we used bimane fluorescence quenching by Trp after introducing tryptophan residues in MEK1 (F53W, F83W, and H100W; Fig. 3*A*, purple sticks) and labeled Cys-less R169E with introduced cysteines (Y173C, T183C, and L300C) using bimane (Fig. 3*B*, orange sticks). We selected these residues based on the HDX-MS data, except for H100W in MEK1. We did not introduce tryptophan into the glycine-rich loop because the introduction might have hindered the binding of AMP-PNP. Instead, we replaced H100, which is close to the glycine-rich loop, with tryptophan (Fig. 3*A*). These mutants did not affect the interaction between the MEK1 and Arr2, suggesting their functional integrity (*SI Appendix*, Fig. S4*B*).

Among all the analyzed Trp-bimane pairs, we detected reduced bimane fluorescence only when MEK1 H100W was coincubated with bimane-labeled Y173C_Arr2 (Fig. 3 *C*–*E*). These results suggest that the interdomain loop I near Y173 of arrestin-2 is close to that of MEK1 H100. As we did not detect decreased HDX levels at H100, but instead at the glycine-rich loop (Fig. 3*A*), interdomain loop I likely binds near the glycine-rich loop of MEK1. The glycine-rich loop is also called the p-loop, as this loop interacts with the phosphate groups of ATP (Fig. 3*A*). As we detected HDX changes only when MEK1 was in complex with AMP-PNP, it is possible that ATP binding maintained the correct conformation of the glycine-rich loop to allow this region to interact with arrestin-2.

To further study the interaction of interdomain loop I and the MEK1 N domain, we incorporated TMSF into Y173 of arrestin-2 (173TMSF) and analyzed ^{1}H-NMR spectra before and after coincubation with MEK1. A notable upfield NMR shift at the 173TMSF site was observed upon coincubation with MEK1 (Fig. 3*F*), suggesting a localized increase in the electronic field at this position, likely due to the interaction with the negatively charged residues in MEK1. The surface charge distribution of MEK1 revealed that negative surface charges are localized near the glycine-rich loop (Fig. 3*G*), further supporting that Y173 of arrestin-2 is closely located to the glycine-rich loop of MEK1.

Binding Interfaces between Arrestin-2 and cRaf. We also investigated the binding interfaces between arrestin-2 and cRaf, the MAP3K of the ERK1/2 cascade. Raf proteins consist of Ras-binding domain (RBD), C1 domain, hinge region, and kinase domain (45, 46). It has been previously reported that the RBD of cRaf is the major binding site for arrestin-2 (27). The expression and purification of full-length cRaf were not successful; therefore, we used cRaf RBD to identify the binding interfaces between arrestin-2 and cRaf. We analyzed the changes in HDX upon coincubation with cRaf RBD and arrestin-2. The HDX-MS results are summarized in Datasets S1 and S4.

HDX-MS analysis showed that the HDX profiles of cRaf RBD were similarly affected by coincubation with both arrestin-2 WT and R169E (Fig. 4*A*, blue ribbon; *SI Appendix*, Fig. S2*C*), suggesting that arrestin-2 activation is not required for cRaf binding. This was confirmed by the cellular BRET assay, which showed that cRaf binding was not affected by Ang II treatment (*SI Appendix*, Fig. S3*C*). Arrestin-2 coincubation reduced HDX within broad regions of the cRaf RBD, with residues 83 to 96 being most significantly affected (Fig. 4*A* and *SI Appendix*, Fig. S2*C*). This result strongly suggests that residues 83 to 96 serve as the binding interface for arrestin-2 interaction. Coincubation of cRaf RBD reduced HDX in only the back loops of both WT and R169E (Fig. 4*B*, blue ribbon; *SI Appendix*, Fig. S2*C*, peptide 305 to 313), suggesting that the back loop is the cRaf binding site.

To confirm that residues 83 to 96 of cRaf and the back loop of arrestin-2 are closely located within the complex, we again employed bimane fluorescence quenching by Trp after introducing tryptophan residues into cRaf (F61W, M76W, and L91W; Fig. 4*A*, purple sticks) and labeling the Cys-less R169E mutant with a single cysteine (E313C_Arr2) with bimane (Fig. 4*B*, orange stick). These mutants did not affect the interaction between the cRaf RBD and Arr2, suggesting their functional integrity (*SI Appendix*, Fig. S4*C*). Coincubation with WT cRaf RBD increased bimane fluorescence compared to that of the buffer control (Fig. 4*C*). Bimane fluorescence intensity is affected by the environment: a hydrophobic environment increases it, whereas a hydrophilic environment decreases it. Therefore, the increase in bimane fluorescence induced by coincubation with WT cRaf RBD may reflect the low exposure of labeled bimane to the buffer upon coincubation with WT cRaf RBD. Among the Trp mutants, although coincubation with cRaf RBD L91W had a major effect on the bimane fluorescence of E313C_Arr2, F61W and M76W also reduced bimane fluorescence of E313C_Arr2 (Fig. 4*C*), suggesting that E313 of arrestin-2 is closely located to F61, M76, and L91 of cRaf, and the distance between cRaf L91 and arrestin-2 E313 is the shortest.

To provide further structural insights into the interaction between cRaf RBD and arrestin-2, we incorporated TMSF into E313 of arrestin-2 (313TMSF). We employed ^{1}H-NMR spectroscopy to monitor the cRaf RBD binding-induced conformational changes in arrestin-2. A notable downfield NMR shift at the 313TMSF site was observed upon coincubation with cRaf RBD (Fig. 4*D*), suggesting a localized decrease in the electronic field at this position, likely due to the interaction with the positively charged residues in cRaf RBD. The surface charge distribution of cRaf RBD revealed that positive surface charges are localized where we observed reduced HDX levels (Fig. 4 *A* and *E*). These results confirmed that the back loop of arrestin-2 interacted with cRaf RBD near residues 83 to 96. Interestingly, the high-resolution structure of the back loop is not significantly different between the basal and activated arrestins (*SI Appendix*, Fig. S1*D*), which explains why both basal and preactivated arrestin-2 interact with cRaf RBD.

Discussion

Previous studies have indicated that activation of arrestin by GPCRs is essential for regulating ERK signaling (41, 47–51). The present study suggested that arrestin activation is essential for its interaction with MEK1 and ERK2 but not with cRaf. We also identified binding interfaces between arrestin-2 and ERK2 signaling components, using a combination of complementary techniques. Based on these data, we propose a working hypothesis for the scaffolding mechanism of arrestin-2 in the ERK2 signaling cascade (Fig. 5*A*).

As cRaf can interact with either basal or activated arrestin-2, cRaf may bind arrestin-2 even before it is activated by a receptor (Fig. 5 *A*, *i* and *ii*). The major binding interface is the RBD of cRaf and the back loop of arrestin-2. In the basal state, the kinase domain of cRaf is blocked by interaction with the N-terminal elements of cRaf, including the RBD and C1 domains (Fig. 5 *B*, *Left*) (52, 53). When other binding proteins, such as GTP-bound Ras, interact with the N-terminal domains, the kinase domain is released and can phosphorylate downstream proteins (52, 53). Thus, it is tempting to speculate that the

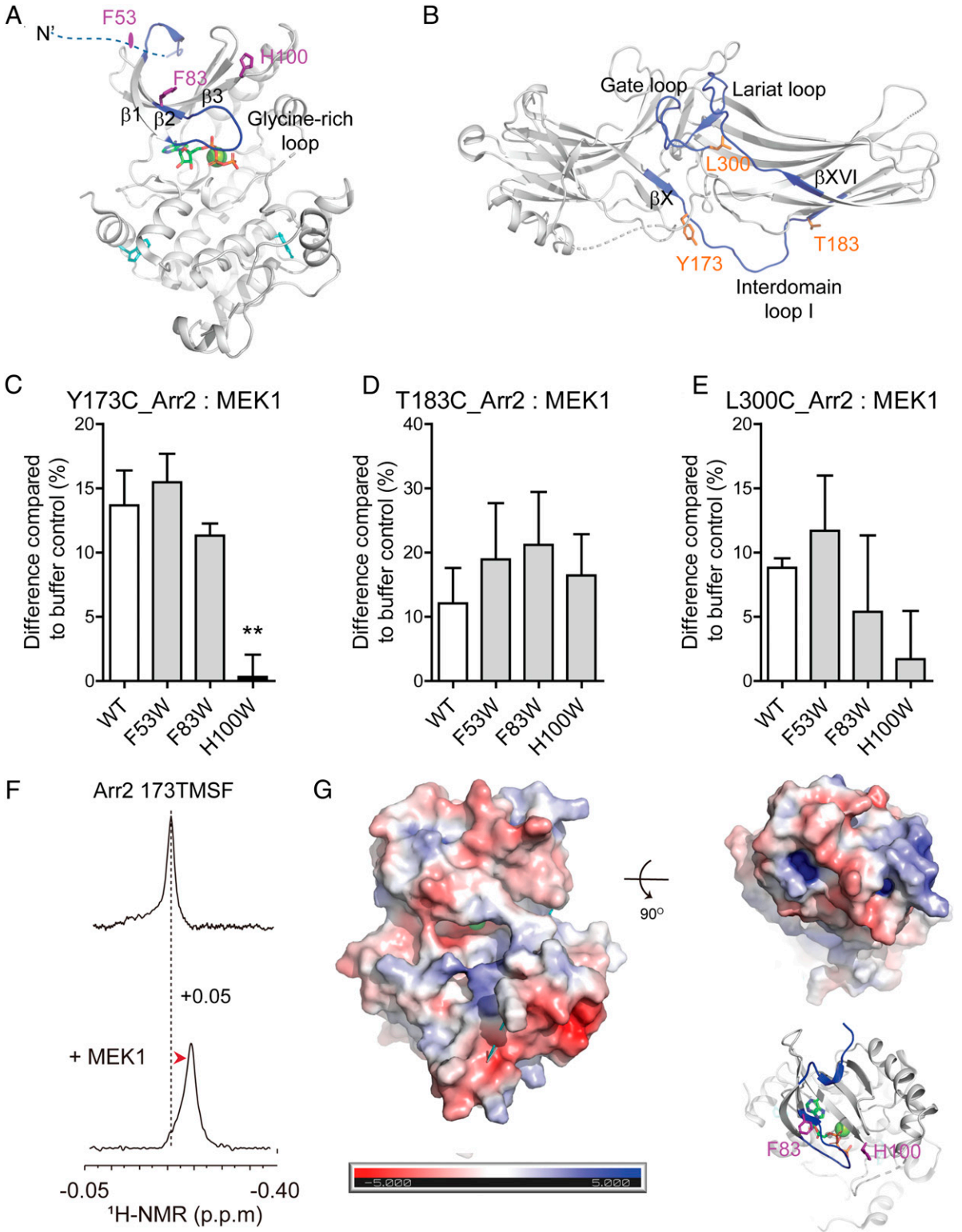

Fig. 3. Interaction of MEK1 and R169E detected by HDX-MS, Trp-induced bimane fluorescence quenching, and ^{1}H-NMR. (*A*) Changes in the HDX profile of AMP-PNP-liganded MEK1 upon coincubation with R169E. Regions with reduced HDX are colored blue on the X-ray crystal structure of MEK1 (PDB: MEK1). The deuterium uptake plots with reduced HDX are shown in *SI Appendix*, Fig. S2*B*. ATP is shown as sticks, and Mg^{2+} is shown as a ball. (*B*) Changes in the HDX profile of R169E upon coincubation with AMP-PNP-liganded MEK1. Regions with reduced HDX are colored blue on the X-ray crystal structure of bovine arrestin-2 (PDB: 1G4R). The deuterium uptake plots with reduced HDX are summarized in *SI Appendix*, Fig. S2*B*. (*C*–*E*) Trp-induced bimane fluorescence quenching upon binding of AMP-PNP-liganded MEK1 and Y173C_Arr2 (*C*), T183C_Arr2 (*D*), and L300C_Arr2 (*E*). Tryptophan residues introduced into MEK1 are depicted by purple sticks, and endogenous tryptophan residues are shown by cyan sticks in *A*. Bimane-labeled cysteines in arrestin-2 are depicted by orange sticks in *B*. Data are from three independent experiments. Error bars indicate SEM. Black bars indicate statistically significant differences from WT, and gray bars indicate the absence of statistically significant difference from WT. *$P < 0.05$, **$P < 0.01$, and ***$P < 0.001$, as compared with coincubation with the WT. (*F*) Effect of MEK1 binding on the ^{1}H-NMR spectrum of 173TMSF incorporated into R169E. (*G*) Surface charge distribution of MEK1. The surface charge was analyzed with adaptive Poisson-Boltzmann solver (APBS) electronics, a PyMOL plugin program, using the MEK1 crystal structure (PDB: MEK1).

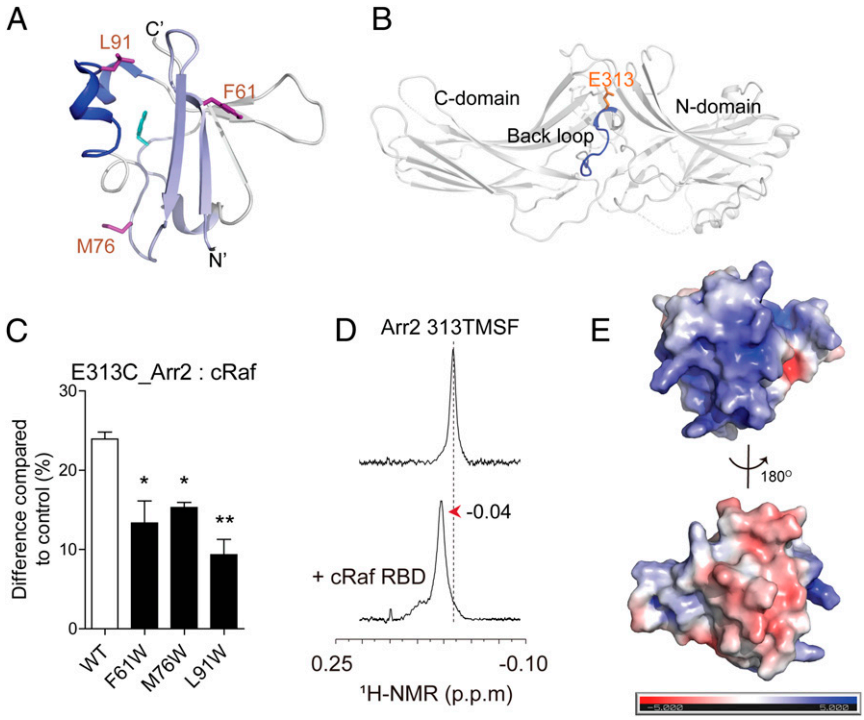

Fig. 4. Interaction of cRaf RBD and R169E detected by HDX-MS, Trp-induced bimane fluorescence quenching, and ^{1}H-NMR. (*A*) Changes in the HDX profile of cRaf RBD upon binding to arrestin-2. Regions with reduced HDX are colored blue on the X-ray crystal structure of cRaf RBD (PDB: 4G3X). The deuterium uptake plots with reduced HDX are summarized in *SI Appendix*, Fig. S2*C*. (*B*) Changes in the HDX profile of arrestin-2 upon binding to cRaf RBD. Regions with reduced HDX are colored blue on the X-ray crystal structure of bovine arrestin-2 (PDB: 1G4R). The deuterium uptake plots with reduced HDX are summarized in *SI Appendix*, Fig. S2*C*. (*C*) Bimane fluorescence quenching by Trp in cRaf RBD with E313C_Arr2. Positions of incorporated tryptophan residues in cRaf RBD are shown by purple sticks, and endogenous tryptophan is shown by cyan stick in *A*. Bimane-labeled Cys residues in arrestin-2 are depicted by orange sticks in *B*. Data are from three independent experiments. Error bars indicate SEM. Black bars indicate statistically significant differences from the WT. $*P < 0.05$, $**P < 0.01$, and $***P < 0.001$, as compared to WT. (*D*) Effect of cRaf RBD binding on the ^{1}H-NMR spectrum of 313TMSF incorporated into R169E. (*E*) Surface charge distribution of cRaf RBD. The surface charge was analyzed with adaptive Poisson-Boltzmann solver (APBS) electronics, a PyMOL plugin program, using the cRaf RBD crystal structure (PDB: 4G3X).

binding of arrestin-2 to the RBD of cRaf may release the kinase domain to facilitate the phosphorylation of MEK1. To test this hypothesis, we analyzed intramolecular BRET by labeling N terminus of cRaf with Rluc and the kinase domain of cRaf with FlAsH, which monitors replacement of the autoinhibitory domain (Fig. 5*B*). Overexpression of arestin-2 reduced the BRET ratio, implying the separation between the autoinhibitory domain and the kinase domain of cRaf in response to arrestin-2 binding. This result supports the hypothesis that arrestin-2 releases the autoinhibitory domain of cRaf from the kinase domain.

Unlike cRaf, MEK1 binds to arrestin-2 only when arrestin-2 is activated, and MEK1 binds more strongly to arrestin-2 when it is bound to ATP (Fig. 5 *A*, *iii*). The interdomain loop I of arrestin-2 is the binding site for the N-lobe of MEK1, which likely orients MEK1 to lower part arrestin-2 (Fig. 5 *A*, *iii*). Since the RBD of cRaf interacts with the back loop of arrestin-2, the released kinase domain may also be located on the same side of arrestin-2 (Fig. 5 *A*, *iii*). In this model, the cRaf kinase domain is located favorably for MEK1 phosphorylation (Fig. 5 *A*, *iii*).

ERK2 also interacted with activated arrestin-2, but the binding was stronger when ERK2 was not ligated with ATP (Fig. 5 *A*, *iv*). This suggests that fully activated ERK2 (dual-phosphorylated and ATP-bound) may easily detach from arrestin-2 to phosphorylate its substrates. In contrast, MEK1 may bind to arrestin-2 when it is fully activated. As we did not test effects of the phosphorylation status of MEK1 or ERK2 on arrestin-2 binding, further investigation is required. Our study suggests that the gate loop of arrestin-2 interacts near the N-lobe of ERK2, whereas the interdomain loop II interacts near the C-lobe of ERK2. The interdomain loop I is on the C-domain side, and the interdomain loop II is on the N-domain side (Fig. 1*A*). Thus, it is likely that ERK2 is located on one side of arrestin-2, while MEK1 is located on the other, so that these two kinases face each other, which likely allows MEK1 easy access to phosphorylate ERK2 (Fig. 5 *A*, *iv*).

A few studies have proposed binding interfaces between arrestin and ERK cascade components (27, 28, 54–56). Xu et al. suggested that the lariat loop through the gate loop of arrestin-3 is a potential binding site for ERK2 (56). Bourquard et al. predicted that the N-lobe of ERK1 interacts with the gate loop of arrestin-2 (27). These results are consistent with our data, which suggest that the gate loop of arrestin-2 is a potential binding site for the N-lobe of ERK2. However, neither of the previous studies proposed that the interdomain loop II of arrestin-2 interacts with the C-lobe of ERK2, although Bourquard et al. suggested that the C-tail of arrestin-2 may interact with ERK2 (27).

Our identification of the binding interface between cRaf and arrestin-2 is consistent with previous reports. Coffa et al. reported that the arrestin-2 R307A mutant failed to interact with cRaf (28), and a molecular simulation study by Bourquard et al. suggested that a region near R307 of arrestin-2 interacted with a region near K84 of cRaf (27). R307 of arrestin-2 and K84 of cRaf were located within the peptides that showed decreased HDX upon coincubation with arrestin-2 and cRaf RBD (*SI Appendix*, Fig. S2*C*). Our data confirm these previous reports and further suggest that arrestin activation is not required for cRaf binding.

Although previous reports of cRaf or ERK2 are consistent with our current results, those of MEK1 are not. Meng et al. suggested that D26 and D29 in the N domain of arrestin-2 and

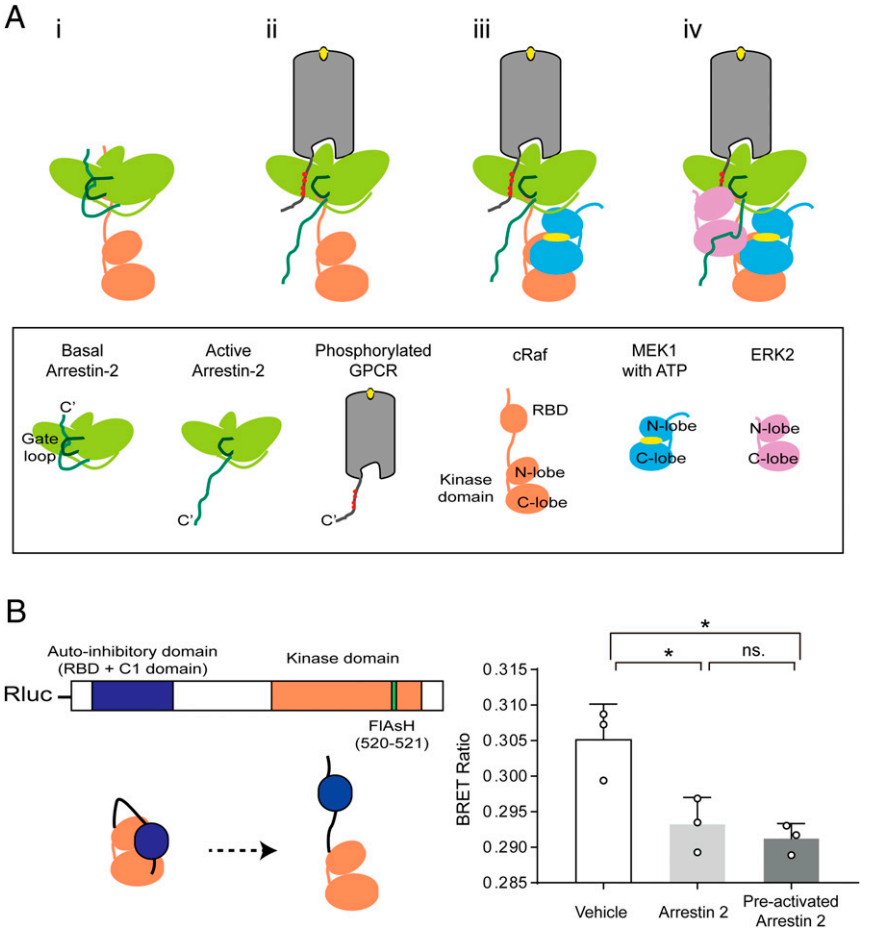

Fig. 5. Proposed model for the scaffolding mechanism of arrestin-2 in the ERK1/2 signaling cascade. (*A*) Summary cartoon illustrating the proposed scaffolding mechanism of arrestin-2 for ERK1/2 signaling components. (*B*) Conformational changes in cRaf upon arrestin-2 binding. The separation between N-terminal region and the kinase domain of cRaf was monitored by intramolecular BRET. Statistical differences between control (no arrestin-2 transfected) and inactive or active arrestin-2 existence were determined by two-sided one-way ANOVA (*$P < 0.05$; **$P < 0.01$; ***$P < 0.001$). n.s., not significant.

residues 46 to 70 in the N-terminal part of MEK1 are critical for the interaction (55); additionally, a molecular simulation study by Bourquard et al. suggested that D29 and E35 of arrestin-2 interacts with a region near E272 of MEK1 (27). Our results suggest that the interdomain loop I of arrestin-2 interacts with the N-lobe of MEK1. This discrepancy may be because Meng et al. used peptide arrays, rather than whole proteins, to define the binding interfaces, and the D26A/D29A mutant of arrestin-2 that they used may have caused an altered conformation (55).

Although we have provided the binding modes between arrestin-2 and each ERK2 signaling component, we did not test whether the binding of one component affects that of others. Previously, Lefkowitz et al. showed that simultaneous expression of either MEK1 or ERK2 with cRaf had no effect on cRaf interaction with arrestin-3 and that simultaneous expression of MEK1 and ERK2 did not affect the interaction of either kinase with arrestin-3 (50). On the other hand, in the same study, coexpression of cRaf enhanced the binding of MEK1 or ERK2 to arrestin-3 (50), and the authors suggested that binding of cRaf to arrestin-3 facilitates the assembly of ERK2 signaling components on arrestin. Since we could not obtain the full-length cRaf, we did not pursue this; further sophisticated studies are needed to investigate whether the binding of one component promotes binding of other ERK2 signaling components.

JNK is another MAPK family member that uses arrestin as a scaffolding protein. Unlike that for ERK signaling, arrestin activation is not required for scaffolding of JNK signaling components (43, 57). Thus, the scaffolding mechanism of JNK through arrestin may differ from that of ERK. Previously, Xu et al. reported that arrestin-3 mutants (K285A/R286A or K295A) that showed reduced ERK2 binding could still interact with JNK3 in a manner similar to that of WT arrestin-3 (56). A few studies, including our recent study, have identified the binding interfaces between arrestin and the components of the JNK activation cascade (26, 29). These studies proposed that β-strand I of arrestin-3 is the major binding site for JNK3, which is different from the binding site of arrestin-2 for ERK2, as suggested by our data. The binding mode and binding site within arrestin-3 for ASK1 (MAP3K for JNK3 signaling cascade) and MKK4/7 (MAP2K for the JNK3 signaling cascade) are also different from those proposed for arrestin-2 and cRaf or MEK1 binding (26). Thus, the data suggest that arrestin-mediated scaffolding of the ERK signaling cascade is mechanistically different from that of the JNK3 signaling cascade, which could pave the way for the selective regulation of arrestin-mediated ERK or JNK signaling.

In summary, we proposed a binding mode between arrestin-2 and components of the ERK2 activation cascade. We identified the positions of arrestin-2 binding sites for cRaf, MEK1, and ERK2 (Fig. 5*A*). Importantly, our finding that ATP binding weakens ERK2 interaction with arrestin-2 suggests that MEK1-phosphorylated ERK2 likely dissociates from arrestin-2, freeing up the site for another molecule of inactive ERK2. This

mechanism would yield signal amplification at this step, similar to that proposed for JNK3 activation on the arrestin-3 scaffold (26). Thus, despite the difference in binding sites, this part of the mechanism of arrestin-mediated scaffolding of MAPK cascades appears to be conserved.

Materials and Methods

Protein Expression and Purification. Complementary deoxyribonucleic acids (cDNAs) of *Rattus norvegicus* (Rat) arrestin-2, human ERK2, human MEK1, and human cRaf RBD were inserted into a pET28a vector containing a hexahistidine tag at the N terminus. For Trp-induced bimane fluorescence quenching experiments, Cys-less arrestin-2 (details described in *Cys-Less Arrestin-2 Generation*) was cloned into the pET22b vector, which contained a hexahistidine tag at the C terminus. The preactivated arrestin-2 mutants (arrestin-$2^{1–384}$, R169E) were generated using the QuikChange Mutagenesis Kit according to the manufacturer's instructions. The constructs were cloned into *Escherichia coli* BL21 (DE3) cells. The transformed cells were grown in Terrific Broth (TB) at 37 °C until the optical density 600 (OD_{600}) reached 0.4 to 0.6. Protein expression was induced with 0.03 mM isopropyl β-d-1-thiogalactopyranoside (IPTG) for 24 h at 16 °C for arrestin-$2^{1–384}$, R169E, and cRaf RBD, with 0.5 mM IPTG for 4 h at 30 °C for ERK2, and with 0.5 mM IPTG for 4 h at 25 °C for MEK1. Harvested cells were resuspended in lysis buffer (arrestin-$2^{1–384}$, R169E, ERK2, and C-Raf RBD; 20 mM Tris HCl pH 7.4, 500 mM NaCl, 10 μg/mL benzamidine, 2.5 μg/mL leupeptin, 100 μM Tris [2-carboxyethyl] phosphine hydrochloride [TCEP], and PIC, MEK1; 50 mM Hepes pH 7.4, 300 mM NaCl, 20 mM $MgCl_2$, 10 μg/mL benzamidine, 2.5 μg/mL leupeptin, 100 μM TCEP, and PIC). Then, 10% glycerol and 5 mg/mL lysozyme were added, and the bacterial cell lysates were incubated for 30 min at room temperature, after which 10 μg/mL DNase I was added, followed by incubation for 30 min at room temperature. The lysates were centrifuged at 13,000 × *g* for 20 min at 4 °C, and the supernatants were collected and loaded into a Ni-NTA column preequilibrated with lysis buffer supplemented with 20 mM imidazole. After binding, the resin was extensively washed with a wash buffer (arrestin-$2^{1–384}$, R169E, ERK2, cRaf RBD; 20 mM Tris HCl pH 7.4, 500 mM NaCl, 20 mM imidazole, 10 μg/mL benzamidine, 2.5 μg/mL leupeptin, 100 μM TCEP, and PIC, MEK1; 50 mM Hepes pH 7.4, 300 mM NaCl, 20 mM $MgCl_2$, 20 mM imidazole, 10 μg/mL benzamidine, 2.5 μg/mL leupeptin, 100 μM TCEP, and PIC). The bound proteins were eluted with an elution buffer (arrestin-$2^{1–384}$, R169E, ERK2, cRaf RBD; 20 mM Hepes pH 7.4, 150 mM NaCl, 400 mM imidazole, 10 μg/mL benzamidine, 2.5 μg/mL leupeptin, 100 μM TCEP, and PIC, MEK1; 50 mM Hepes pH 7.4, 100 mM NaCl, 20 mM $MgCl_2$, 400 mM imidazole, 10 μg/mL benzamidine, 2.5 μg/mL leupeptin, 100 μM TCEP, and PIC). The Ni-NTA purified fractions were loaded onto a Superde200 Increase 10/300 GL column in an ÄKTA fast protein liquid chromatography (FPLC) system (GE Healthcare Life Science). Protein elution was monitored at 280 nm, and the protein-containing fractions were collected.

Coincubation Protocol. The purified proteins were prepared in a buffer containing 20 mM Hepes pH 7.4 and 150 mM NaCl. The proteins were concentrated using a Vivaspin 500, 10 kDa molecular weight cutoff (GE Healthcare Life Science). To form arrestin-$2^{1–384}$/ERK2 complex or R169E/MEK1 complex, proteins were mixed at a final concentration of 40 μM. R169E and cRaf RBD were mixed in two conditions (40 μM R169E and 80 μM cRaf RBD or 80 μM R169E and 40 μM cRaf RBD). All the complexes were allowed to form at room temperature for 2 h.

HDX-MS. For arrestin-$2^{1–384}$/ERK2 and R169E/MEK1 complexes, HDX was initiated by mixing 3 μL of the protein samples and 27 μL D_2O buffer (20 mM Hepes pD 7.4, 150 mM NaCl, and 10% glycerol in D_2O), and incubated for 10, 100, 1,000, or 10,000 s at 4 °C. The mixtures were quenched by the addition of 30 μL ice-cold quench buffer (100 mM NaH_2PO_4 pH 2.01 and 20 mM TCEP). For nondeuterated samples (ND), 3 μL of the protein samples were mixed with 27 μL H_2O buffer (20 mM Hepes pH 7.4, 150 mM NaCl, and 10% glycerol in H_2O) and quenched with 30 μL ice-cold quench buffer. For R169E/cRaf RBD complex in a 1:2 ratio, HDX was initiated by mixing 5 μL complex and 25 μL D_2O buffer, incubated for 10, 100, 1,000, or 10,000 s at 4 °C, and quenched with 30 μL ice-cold quenching buffer. For ND samples, 5 μL complex was mixed with 25 μL H_2O buffer and quenched with 30 μL ice-cold quench buffer. For R169E/cRaf RBD complex in a 2:1 ratio, 7 μL complex was mixed with 23 μL D_2O buffer, incubated for 10, 100, 1,000, or 10,000 s at 4 °C, and quenched with 30 μL ice-cold quench buffer. For ND, 7 μL complex was mixed with 23 μL H_2O buffer and quenched with 30 μL ice-cold quench buffer.

The quenched samples were digested by passing through an immobilized pepsin column (2.1 × 30 mm; Life Technologies) at a flow rate of 100 μL/min with 0.05% formic acid in H_2O at 12 °C. Peptide fragments were subsequently collected on a C18 VanGuard trap column (1.7 μm × 30 mm; Waters) for desalting with 0.05% formic acid in H_2O. Peptic peptides were then separated with ultrapressure liquid chromatography on an ACQUITY ultraperformance liquid chromatography (UPLC) C18 column (1.7 μm, 1.0 × 100 mm; Waters) at 40 μL/min with an acetonitrile gradient created by two pumps: mobile phase A (0.15% formic acid in H_2O) and B (0.15% formic acid in acetonitrile). The gradient started with 8% B and increased to 85% B over the next 8.5 min. To minimize the back exchange of deuterium to hydrogen, the sample, solvents, trap, and UPLC column were all maintained at pH 2.5 and 0.5 °C during analysis. MS analyses were performed using a Xevo G2 quadrupole time-of-flight (QTof) equipped with a standard electrospray ionization source (Waters). The mass spectra were acquired in the range of *m/z* 100 to 2,000 for 12 min in positive ion mode. Peptides were identified in ND samples with ProteinLynx Global Server 2.4 (Waters). The following parameters were applied: monoisotopic mass, nonspecific for the enzyme while allowing up to one missed cleavage, MS/MS ion searches, automatic fragment mass tolerance, and automatic peptide mass tolerance. Searches were performed with the variable methionine oxidation modification, and the peptides were filtered with a peptide score of 6. To process the HDX-MS data, the amount of deuterium in each peptide was determined by measuring the centroid of the isotopic distribution using DynamX 3.0 (Waters).

Cys-Less Arrestin-2 Generation. For Trp-induced bimane fluorescence quenching experiments, the seven native cysteine residues (C69, C125, C140, C150, C242, C251, and C270) of arrestin-2 were mutated to alanine to generate Cys-less arrestin-2. Then, preactivated arrestin-2 (arrestin-$2^{1–384}$, R169E) was generated. For bimane labeling, a cysteine residue was introduced into the Cys-less arrestins, resulting in six engineered arrestin constructs (arrestin-$2^{1–384}$; L300C and P356C, R169E; Y173C, T183C, L300C, and E313C). In conjunction with bimane labeling of cysteines, a tryptophan residue was introduced into ERK2, MEK1, and cRaf RBD, resulting in six engineered ERK2 constructs (V47W, Y62W, Y111W, H123W, F226W/Y231W, and L265W), three engineered MEK1 constructs (F53W, F83W, and H100W), and three engineered cRaf RBD constructs (F61W, M76W, and L91W). All mutagenesis was performed using the QuikChange Mutagenesis Kit.

Trp-Induced Bimane Fluorescence Quenching. WT ERK2, MEK1, cRaf RBD, and their tryptophan mutants were purified and exchanged into an interaction buffer (ERK2: 10 mM Hepes pH 7.4 and 150 mM NaCl; MEK1 and cRaf RBD: 20 mM Hepes pH 7.4, 150 mM NaCl). Cys-less arrestin-$2^{1–384}$ or Cys-less R169E was purified and replaced with a labeling buffer (ERK2: 10 mM MES pH 6.5 and 150 mM NaCl; MEK1 and cRaf RBD: 20 mM MES pH 6.5 and 150 mM NaCl). Cys-less arrestin-$2^{1–384}$ or Cys-less R169E were concentrated to 50 μM and labeled with bimane to a final concentration of 0.5 mM. Excess dye was removed through another cycle of buffer exchange into the interaction buffer after 3 h of incubation at room temperature. ERK2 signaling components and Cys-less arrestin-$2^{1–384}$ or Cys-less R169E were mixed at 2 μM in 100 μL interaction buffer for 30 min at room temperature, and the samples were placed in a MicroFluor 96-well fluorescent plate. The samples were excited at 390 nm, and the emitted fluorescence was measured from 420 to 600 nm using a 10-nm step size. Each data point was integrated for 0.2 s for ERK2 and 0.1 s for MEK1 and RBD. The spectra were analyzed using GraphPad Prism 7.

Unnatural Amino Acid Incorporation. Unnatural amino acids were incorporated into arrestin-2 via genetic code expansion as previously described (58, 59). The L300TAG or E313TAG of arrestin-2 in pET-22b was transformed into BL21(DE3) cells with pEVOL-TMSFRS. Cells were induced by the addition of 0.02% L-arabinose, 0.5 mM TMSF, and 0.2 mM IPTG after growing in TB medium, containing 100 μg/mL ampicillin and 50 μg/mL chloramphenicol, to an OD = 0.8 for 16 h at 25 °C. Harvested *E. coli* cell pellets were resuspended in buffer (20 mM Tris HCl, pH 8.0, and 150 mM NaCl) and lysed by homogenization (JN-3000 PLUS, JNBIO). The supernatant was incubated with Ni-NTA resin for 2 h at 4 °C, and the TMSF-incorporated arrestin-2 was eluted with lysis buffer containing 250 mM imidazole. The protein was further purified using a size-exclusion column (Superdex 200 increase, GE Healthcare). Similar procedures were performed to obtain F2Y-incorporated arrestin-2, using the plasmids H362TAG arrestin-2 and pEVOL-F2YRS. Cells were induced 0.02% L-arabinose, 0.5 mM TMSF, and 0.2 mM IPTG instead.

^{19}F-NMR and ^{1}H-NMR. TMSF-incorporated arrestin-2 was diluted to 10 μM in buffer (20 mM HCl pH 8.0 and 150 mM NaCl) containing 10% (volume/volume) D_2O with or without incubating with 10 μM ERK2, MEK1, or cRaf RBD for 30 min at room temperature. One-dimensional (1D) ^{1}H-NMR spectra were recorded for 18 min at 25 °C using an Avance 950 MHz spectrometer

with a cryoprobe, which is a proton-optimized triple resonance (Bruker). Spectra were analyzed using the program ZGGPW5 (NS = 510, DS = 4, SW = 16 part per million (ppm), AQ = 1.93 s, D1 =1.5 s), and the chemical shifts of the peaks were determined by referring to D_2O (4.69 ppm). 50 μM arrestin-2 362F2Y was subjected to NMR before and after incubation with 50 μM ERK2. Spectra were recorded by an Agilent 500 MHz spectrometer, scanning 15,000 times with a recovery delay of 1.5 s. Data were processed using 20-Hz Lorentzian line broadening, and the chemical shift was determined by referring to the TFAb (−76.5 ppm).

GST Pull-Down Assay. Arrestin-2 WT and cystine mutants were cloned to pGEX-6p-2 vector and overexpressed in *E. coli*. A total of 1 μM His-tagged MAPKs WT and mutants were mixed with 15 μL GST resin for 2 h in 4 °C with or without the preincubation of 1 μM arrestin-2 proteins. The GST beads were collected by centrifuge at 800 × *g* and washed with wash buffer (binding buffer with 0.5% Tween20) four times. After removing the supernatant, the samples were resuspended in 50 μL 2× sodium dodecyl sulfate (SDS) loading buffer and boiled for 10 min before Western blot. Antibodies including anti-GST (Cell Signaling Technology, catalog no. 2622) and anti-His (Cell Signaling Technology, catalog no. 2366) were used. The data were analyzed using the Image J (version 1.8.0) and GraphPad Prism 7.0 software.

BRET Assay. The BRET assay was designed to examine the interaction between MAPKs and arrestin-2 (60, 61). The FlAsH-BRET sensor for cRaf, MEK1, and ERK2 was generated by inserting the FlAsH-EDT_2 binding motif, CCPGCC, into the specific sites of cRaf (89 CCPGCC 90), MEK1 (100 CCPGCC 101), and ERK2 (122 CCPGCC 123) in the pcDNA 3.1, which encodes these kinases. Angiotensin II receptor type 1 (AT1R), arrestin-2-Rluc, CCPGCC-inserted ERK2, MEK1, and cRaf were cotransfected into HEK 293A cells in 6-well plates. 48 h posttransfection, cells were seeded into 96-well culture plates, at a density of 3×10^4 cells per well. In total, 10 μM FlAsH-EDT2 was added to each well, and the cells were incubated at 37 °C in 5% CO_2 for 40 min. Cells were washed with BRET buffer (25 mM Hepes pH 7.5, 1 mM $CaCl_2$, 140 mM NaCl, 2.7 mM KCl, 0.9 mM $MgCl_2$, 0.37 mM NaH_2PO_4, 5.5 mM D-Glucose, 12 mM $NaHCO_3$) twice and incubated with the required substrate (coelenterazine-h for Rluc-arrestin-2) at a concentration of 5 μM in the presence or absence of 10 μM angiotensin II. Luciferase (440 to 480 nm) and FlAsH (525 to 585 nm) emissions were detected using a Multimode Plate Reader (PerkinElmer EnVision) at 25 °C immediately after substrate addition. The BRET ratio was calculated by dividing the 535-nm emission by the 460-nm emission.

Intramolecular BRET assay to examine the effect of arrestin-2 in the release of the autoinhibition among cRaf was done using HEK293A cells. Cells were seeded in 6-well plates after being transfected with Rluc-c-Raf-1 V520-CCPGCC-D521 with or without arrestin-2 using polyethylenimine for 24 h. Then, the cells were distributed into 96-well plates at a density of ∼25,000 cells per well. After another 24-h incubation at 37 °C, the cells were labeled FlAsH-EDT2 (2.5 μM) for 40 min at 37 °C and washed twice with BRET buffer (25 mM Hepes pH 7.4, 140 mM NaCl, 2.7 mM KCl, 1 mM CaCl2, 12 mM $NaHCO_3$, 5.6 mM D-glucose, 0.5 mM $MgCl_2$, and 0.37 mM NaH_2PO_4) and stimulated with or without isoproterenol (final concentration of 20 μM) at 37 °C for 15 min. Luciferase substrate coelenterazine-h was added at a final concentration of 5 μM. The BRET signal was determined by calculating the ratio of the light intensity emitted by FlAsH (530/20 nM) over the light intensity emitted by Rluc (485/20 nM). The data were analyzed by GraphPad Prism 7.0 software.

Statistical Analysis. For HDX-MS studies, the Student's *t* test was used to assess the statistically significant differences between samples with and without the binding partner. To analyze differences between more than three conditions, one-way ANOVA followed by Tukey's post hoc test was used. Statistical significance was set at $P < 0.05$. More than three independent experiments were performed on each dataset.

Data Availability. All study data are included in the article and/or supporting information.

ACKNOWLEDGMENTS. We thank Professor Chang-wen Jin and the staff of Beijing NMR Center and the NMR facility of the National Center for Protein Sciences at Peking University for NMR data collection and analysis. This work was supported by grants from the National Research Foundation of Korea funded by the Korean government (NRF-2021R1A2C3003518 and NRF-2019R1A5A2027340 to K.Y.C.) and NIH Grants R35 GM122491, RO1 EY011500 (V.V.G. and T.M.I.), and GM120569 (T.M.I.). We acknowledge support from the National Key R&D Program of China (2018YFC1003600 to J.-P.S.), the National Science Fund for Distinguished Young Scholars (81825022 to J.-P.S.), the National Natural Science Foundation of China (91939301 to J.-P.S. and 32000592 to C.Q.), and the Key Research Program of the Beijing Natural Science Foundation (Z200019 to J.-P.S.).

1. R. Roskoski Jr, ERK1/2 MAP kinases: Structure, function, and regulation. *Pharmacol. Res.* **66**, 105–143 (2012).
2. D. K. Morrison, MAP kinase pathways. *Cold Spring Harb. Perspect. Biol.* **4**, a011254 (2012).
3. W. Peti, R. Page, Molecular basis of MAP kinase regulation. *Protein Sci.* **22**, 1698–1710 (2013).
4. M. D. Brown, D. B. Sacks, Protein scaffolds in MAP kinase signalling. *Cell. Signal.* **21**, 462–469 (2009).
5. W. Kolch, Coordinating ERK/MAPK signalling through scaffolds and inhibitors. *Nat. Rev. Mol. Cell Biol.* **6**, 827–837 (2005).
6. B. H. Lee, P. H. Neela, M. S. Kent, A. M. Zehnder, IQGAP1 is an oncogenic target in canine melanoma. *PLoS One* **12**, e0176370 (2017).
7. T. Chen *et al*., Identification of small-molecule inhibitors of the JIP-JNK interaction. *Biochem. J.* **420**, 283–294 (2009).
8. D. N. Dhanasekaran, K. Kashef, C. M. Lee, H. Xu, E. P. Reddy, Scaffold proteins of MAP-kinase modules. *Oncogene* **26**, 3185–3202 (2007).
9. K. Yoshioka, Scaffold proteins in mammalian MAP kinase cascades. *J. Biochem.* **135**, 657–661 (2004).
10. M. J. Lohse, C. Hoffmann, Arrestin interactions with G protein-coupled receptors. *Handb. Exp. Pharmacol.* **219**, 15–56 (2014).
11. J. S. Smith, S. Rajagopal, The β-arrestins: Multifunctional regulators of G protein-coupled receptors. *J. Biol. Chem.* **291**, 8969–8977 (2016).
12. J. L. Benovic *et al*., Functional desensitization of the isolated beta-adrenergic receptor by the beta-adrenergic receptor kinase: Potential role of an analog of the retinal protein arrestin (48-kDa protein). *Proc. Natl. Acad. Sci. U.S.A.* **84**, 8879–8882 (1987).
13. M. J. Lohse, J. L. Benovic, J. Codina, M. G. Caron, R. J. Lefkowitz, beta-Arrestin: A protein that regulates beta-adrenergic receptor function. *Science* **248**, 1547–1550 (1990).
14. S. A. Vishnivetskiy *et al*., Molecular defects of the disease-causing human arrestin-1 C147F mutant. *Invest. Ophthalmol. Vis. Sci.* **59**, 13–20 (2018).
15. K. A. DeFea, Beta-arrestins as regulators of signal termination and transduction: How do they determine what to scaffold? *Cell. Signal.* **23**, 621–629 (2011).
16. K. Xiao *et al*., Functional specialization of beta-arrestin interactions revealed by proteomic analysis. *Proc. Natl. Acad. Sci. U.S.A.* **104**, 12011–12016 (2007).
17. V. V. Gurevich, E. V. Gurevich, W. M. Cleghorn, Arrestins as multi-functional signaling adaptors. *Handb. Exp. Pharmacol.* **186**, 15–37 (2008).
18. E. V. Gurevich, V. V. Gurevich, Arrestins: Ubiquitous regulators of cellular signaling pathways. *Genome Biol.* **7**, 236 (2006).
19. S. A. Laporte, M. G. H. Scott, β-arrestins: Multitask scaffolds orchestrating the where and when in cell signalling. *Methods Mol. Biol.* **1957**, 9–55 (2019).
20. Z. Zhang, R. W. Vachet, Gas-phase protein salt bridge stabilities from collisional activation and electron transfer dissociation. *Int. J. Mass Spectrom.* **420**, 51–56 (2017).
21. J. H. Dong *et al*., Adaptive activation of a stress response pathway improves learning and memory through Gs and β-arrestin-1-regulated lactate metabolism. *Biol. Psychiatry* **81**, 654–670 (2017).
22. S. Coffa *et al*., The effect of arrestin conformation on the recruitment of c-Raf1, MEK1, and ERK1/2 activation. *PLoS One* **6**, e28723 (2011).
23. E. G. Strungs, L. M. Luttrell, Arrestin-dependent activation of ERK and Src family kinases. *Handb. Exp. Pharmacol.* **219**, 225–257 (2014).
24. P. H. McDonald *et al*., Beta-arrestin 2: A receptor-regulated MAPK scaffold for the activation of JNK3. *Science* **290**, 1574–1577 (2000).
25. Q. Chen *et al*., Structural basis of arrestin-3 activation and signaling. *Nat. Commun.* **8**, 1427 (2017).
26. N. A. Perry *et al*., Arrestin-3 scaffolding of the JNK3 cascade suggests a mechanism for signal amplification. *Proc. Natl. Acad. Sci. U.S.A.* **116**, 810–815 (2019).
27. T. Bourquard *et al*., Unraveling the molecular architecture of a G protein-coupled receptor/β-arrestin/Erk module complex. *Sci. Rep.* **5**, 10760 (2015).
28. S. Coffa, M. Breitman, B. W. Spiller, V. V. Gurevich, A single mutation in arrestin-2 prevents ERK1/2 activation by reducing c-Raf1 binding. *Biochemistry* **50**, 6951–6958 (2011).
29. J. Y. Park *et al*., Structural mechanism of the arrestin-3/JNK3 interaction. *Structure* **27**, 1162–1170.e3 (2019).
30. S. R. Marcsisin, J. R. Engen, Hydrogen exchange mass spectrometry: What is it and what can it tell us? *Anal. Bioanal. Chem.* **397**, 967–972 (2010).
31. S. E. Mansoor, H. S. McHaourab, D. L. Farrens, Mapping proximity within proteins using fluorescence spectroscopy. A study of T4 lysozyme showing that tryptophan residues quench bimane fluorescence. *Biochemistry* **41**, 2475–2484 (2002).
32. W. Huang *et al*., Structure of the neurotensin receptor 1 in complex with β-arrestin 1. *Nature* **579**, 303–308 (2020).
33. X. E. Zhou *et al*., Identification of phosphorylation codes for arrestin recruitment by G protein-coupled receptors. *Cell* **170**, 457–469.e13 (2017).
34. F. Yang *et al*., Phospho-selective mechanisms of arrestin conformations and functions revealed by unnatural amino acid incorporation and (19)F-NMR. *Nat. Commun.* **6**, 8202 (2015).
35. D. P. Staus *et al*., Structure of the M2 muscarinic receptor-β-arrestin complex in a lipid nanodisc. *Nature* **579**, 297–302 (2020).

36. Y. Kang *et al*., Crystal structure of rhodopsin bound to arrestin by femtosecond X-ray laser. *Nature* **523**, 561–567 (2015).
37. A. K. Shukla *et al*., Structure of active β-arrestin-1 bound to a G-protein-coupled receptor phosphopeptide. *Nature* **497**, 137–141 (2013).
38. P. Scheerer, M. E. Sommer, Structural mechanism of arrestin activation. *Curr. Opin. Struct. Biol.* **45**, 160–169 (2017).
39. D. K. Kim, Y. Yun, H. R. Kim, M. D. Seo, K. Y. Chung, Different conformational dynamics of various active states of β-arrestin1 analyzed by hydrogen/deuterium exchange mass spectrometry. *J. Struct. Biol.* **190**, 250–259 (2015).
40. Y. J. Kim *et al*., Crystal structure of pre-activated arrestin p44. *Nature* **497**, 142–146 (2013).
41. E. Cassier *et al*., Phosphorylation of β-arrestin2 at Thr^{383} by MEK underlies β-arrestin-dependent activation of Erk1/2 by GPCRs. *eLife* **6**, e23777 (2017).
42. M. P. Gray-Keller, P. B. Detwiler, J. L. Benovic, V. V. Gurevich, Arrestin with a single amino acid substitution quenches light-activated rhodopsin in a phosphorylation-independent fashion. *Biochemistry* **36**, 7058–7063 (1997).
43. S. Kook *et al*., Arrestin-3 binds c-Jun N-terminal kinase 1 (JNK1) and JNK2 and facilitates the activation of these ubiquitous JNK isoforms in cells via scaffolding. *J. Biol. Chem.* **288**, 37332–37342 (2013).
44. J. Granzin, A. Stadler, A. Cousin, R. Schlesinger, R. Batra-Safferling, Structural evidence for the role of polar core residue Arg175 in arrestin activation. *Sci. Rep.* **5**, 15808 (2015).
45. E. Park *et al*., Architecture of autoinhibited and active BRAF-MEK1-14-3-3 complexes. *Nature* **575**, 545–550 (2019).
46. D. Matallanas *et al*., Raf family kinases: Old dogs have learned new tricks. *Genes Cancer* **2**, 232–260 (2011).
47. S. R. Jung, C. Kushmerick, J. B. Seo, D. S. Koh, B. Hille, Muscarinic receptor regulates extracellular signal regulated kinase by two modes of arrestin binding. *Proc. Natl. Acad. Sci. U.S.A.* **114**, E5579–E5588 (2017).
48. A. Tohgo, K. L. Pierce, E. W. Choy, R. J. Lefkowitz, L. M. Luttrell, beta-Arrestin scaffolding of the ERK cascade enhances cytosolic ERK activity but inhibits ERK-mediated transcription following angiotensin AT1a receptor stimulation. *J. Biol. Chem.* **277**, 9429–9436 (2002).
49. H. Kobayashi, Y. Narita, M. Nishida, H. Kurose, Beta-arrestin2 enhances beta2-adrenergic receptor-mediated nuclear translocation of ERK. *Cell. Signal.* **17**, 1248–1253 (2005).
50. L. M. Luttrell *et al*., Activation and targeting of extracellular signal-regulated kinases by beta-arrestin scaffolds. *Proc. Natl. Acad. Sci. U.S.A.* **98**, 2449–2454 (2001).
51. S. K. Shenoy *et al*., beta-arrestin-dependent, G protein-independent ERK1/2 activation by the beta2 adrenergic receptor. *J. Biol. Chem.* **281**, 1261–1273 (2006).
52. L. Santarpia, S. M. Lippman, A. K. El-Naggar, Targeting the MAPK-RAS-RAF signaling pathway in cancer therapy. *Expert Opin. Ther. Targets* **16**, 103–119 (2012).
53. C. M. Udell, T. Rajakulendran, F. Sicheri, M. Therrien, Mechanistic principles of RAF kinase signaling. *Cell. Mol. Life Sci.* **68**, 553–565 (2011).
54. X. Song, S. Coffa, H. Fu, V. V. Gurevich, How does arrestin assemble MAPKs into a signaling complex? *J. Biol. Chem.* **284**, 685–695 (2009).
55. D. Meng *et al*., MEK1 binds directly to betaarrestin1, influencing both its phosphorylation by ERK and the timing of its isoprenaline-stimulated internalization. *J. Biol. Chem.* **284**, 11425–11435 (2009).
56. T. R. Xu *et al*., Mutations of beta-arrestin 2 that limit self-association also interfere with interactions with the beta2-adrenoceptor and the ERK1/2 MAPKs: Implications for beta2-adrenoceptor signalling via the ERK1/2 MAPKs. *Biochem. J.* **413**, 51–60 (2008).
57. X. Zhan, T. S. Kaoud, K. N. Dalby, V. V. Gurevich, Nonvisual arrestins function as simple scaffolds assembling the MKK4-JNK3α2 signaling complex. *Biochemistry* **50**, 10520–10529 (2011).
58. Q. Liu *et al*., DeSiphering receptor core-induced and ligand-dependent conformational changes in arrestin via genetic encoded trimethylsilyl ^{1}H-NMR probe. *Nat. Commun.* **11**, 4857 (2020).
59. F. Yang *et al*., Allosteric mechanisms underlie GPCR signaling to SH3-domain proteins through arrestin. *Nat. Chem. Biol.* **14**, 876–886 (2018).
60. T. Li *et al*., Homocysteine directly interacts and activates the angiotensin II type I receptor to aggravate vascular injury. *Nat. Commun.* **9**, 11 (2018).
61. F. Yang *et al*., Structural basis of GPBAR activation and bile acid recognition. *Nature* **587**, 499–504 (2020).